RESEARCH ARTICLE

Quantification of H3.1-nucleosomes using a chemiluminescent immunoassay: A reliable method for neutrophil extracellular trap detection

Marion Wargnies[1], Guillaume Rommelaere[1], Julie Candiracci[1], Dorian Pamart[1], Robin Varsebroucq[1], Florian Jibassia[1], Finley Serneo[2], Virginie Laloux[1], Olivia Thiry[1], Fanny Lambert[1], Alison Lobbens[1], Priscilla Van den Ackerveken[1], Marielle Herzog[1]*

1 Belgian Volition SRL, Parc Scientifique Crealys, 22 Rue Phocas Lejeune, Isnes, Belgium, **2** Volition America Inc, Corte Del Cedro, Carlsbad, California, United States of America

* M.Herzog@volition.com

Abstract

Neutrophil extracellular traps (NETs) are chromatin-based web-like structures released by activated neutrophils in response to infectious agents. Overproduction or insufficient clearance of NETs contributes to dysfunction of immune response and disease pathogenesis, underlying the importance of early detection and monitoring of NET levels in clinical samples. While existing methods for NETs detection and quantification face limitations, there is a pressing need for a reliable, sensitive, and clinically applicable assay. Since NETs consist of long strains of decondensed chromatin, with nucleosomes as their basic units, we propose circulating H3.1-nucleosomes as biomarkers for NETs detection in clinical plasma samples. In the initial phase of our study, we confirmed the presence of H3.1-nucleosomes by immunofluorescence and immunoprecipitation experiments in two *in vitro* NET models: neutrophil-like cells differentiated from the HL-60 cell line, and primary neutrophils isolated from whole blood, both treated with either phorbol 12-myristate 13-acetate or calcium ionophore A23187 to induce NETs formation. Subsequently, we developed and analytically validated a chemiluminescent immunoassay for the quantification of circulating H3.1-nucleosomes in plasma. This fully automated assay demonstrates convincing analytical performance in parameters including sensitivity, precision, linearity and reproducibility. Overall, by measuring the H3.1-nucleosome levels in plasma samples from patients suffering from NETs-related diseases compared to healthy donors, we demonstrated the assay's clinical value in identifying NETs-associated pathologies and its potential utility for disease management.

OPEN ACCESS

Citation: Wargnies M, Rommelaere G, Candiracci J, Pamart D, Varsebroucq R, Jibassia F, et al. (2025) Quantification of H3.1-nucleosomes using a chemiluminescent immunoassay: A reliable method for neutrophil extracellular trap detection. PLoS One 20(8): e0329352. https://doi.org/10.1371/journal.pone.0329352

Editor: Zhiming Li, Sichuan University, CHINA

Received: February 11, 2025

Accepted: July 15, 2025

Published: August 6, 2025

Data availability statement: All relevant data are within the manuscript and its Supporting Information files.

Funding: The author(s) received no specific funding for this work.

Competing interests: All authors are employees of VolitionRx Ltd. M.H. is a shareholder of VolitionRx Ltd. This does not alter our adherence to PLOS ONE policies on sharing data and materials.

1. Introduction

Nucleosomes are the basic structural units of chromatin, consisting of DNA wrapped around a core of histone proteins (H2A, H2B, H3, and H4) [1]. In the nucleus, these complexes are involved in chromatin compaction, contributing to gene expression regulation [2,3]. Beyond their intracellular functions, circulating nucleosomes have emerged as significant biomarkers in various pathological conditions due to their association with cellular stress, damage, and death [4–7]. Among the different types of cell death, NETosis appears as a particularly intriguing process [8]. NETosis is a specialized form of programmed cell death of neutrophils, the most abundant circulating white blood cell and the first line of defense in the innate immune response. NETosis results in the release of neutrophil extracellular traps (NETs), which are composed of long stretches (i.e., 15,000–30,000 bp) of decondensed chromatin decorated with granule proteins such as myeloperoxidase (MPO) and neutrophil elastase (NE) [9,10]. Besides the beneficial role of NETs in the defense against pathogens, excess production or dysregulation of NETs release is associated with exacerbated inflammation and organ damage [11–14]. The significant contribution of NETs in various pathologies including sepsis, COVID-19, rheumatoid arthritis, systemic lupus erythematosus, and others [15–25] highlights the importance of detecting and monitoring NET levels in clinical samples [26–28]. Traditionally, NETs are detected using methods such as fluorescence microscopy or enzyme-linked immunosorbent assays (ELISA) targeting NET components such as MPO, cell-free DNA (cfDNA), citrullinated histone H3 (H3Cit), and MPO-DNA complexes [29–34]. Although these methods have been described in the literature to detect NETs *in vitro* and *in vivo*, they have several limitations in clinical applications, particularly regarding sensitivity, standardization and automation. This highlights the need for a robust and analytically validated method for NETs detection in clinical settings [35,36].

Since NETs are composed of decondensed chromatin, and nucleosomes are inherent constituents of this structure, we hypothesize that circulating nucleosomes – particularly those containing the H3.1 histone variant – could serve as biomarkers for NETs detection in clinical samples [37–39]. Investigating nucleosomes offers several advantages over other NET components, such as free histones or cfDNA, due to their inherent structural stability, which protects them from rapid degradation in the bloodstream [4,40]. Additionally, unlike histone post-translational modifications (PTMs) that may be affected by enzymatic activity or clipping events, nucleosomal detection is less influenced by these variables.

In this study, we first confirmed the presence of H3.1-nucleosomes in NETs using two complementary *in vitro* models; the well-established DMSO-differentiated HL-60 cells [41,42] and primary human neutrophils [43], both stimulated by either phorbol 12-myristate 13-acetate (PMA) or calcium ionophore A23187 (CI). Immunofluorescence microscopy confirmed the presence of H3.1-nucleosomes in the NET structures in both models. To further validate these findings, immunoprecipitation (IP) experiments demonstrated the physical association of H3.1-nucleosomes with other NET components in HL-60-derived NETs. These results collectively support the relevance of H3.1-nucleosome quantification as a biomarker for NETs.

Building on this, we developed an automated and standardized chemiluminescent immunoassay (ChLIA) for the detection of circulating H3.1-nucleosomes in plasma samples. This fully automated assay employs an anti-histone H3.1 antibody in capture on the solid phase, consisting of magnetic particles, in combination with a conformational anti-nucleosome antibody coupled with acridinium ester molecules in detection. Analytical validation demonstrated that the assay is highly sensitive, precise, linear, and reproducible.

Finally, we evaluated the clinical utility of this H3.1-nucleosome immunoassay by measuring circulating H3.1-nucleosome levels in plasma samples from patients suffering from diverse NETs-associated diseases compared with healthy donors. The results showed significantly elevated levels of circulating H3.1-nucleosomes in patients with NETs-related diseases compared with the control population, confirming the assay's potential for monitoring NET levels in clinical settings. Overall, this study demonstrates the development of an analytically validated quantitative NETs assay and highlights the strong potential of the H3.1-nucleosome immunoassay as a valuable diagnostic tool for NETs-associated conditions.

2. Materials and methods

2.1. HL-60 cell line culture and NETosis induction

HL-60 cells were purchased from ATCC (CCL240; ATCC; Manassas, USA). The cells were cultured in Iscove's Modified Dulbecco's Medium (IMDM) (31980048; ThermoFisher scientific; Waltham, USA) glutaMAX (31980048; Gibco, ThermoFisher scientific, Waltham, USA) supplemented with 15% fetal bovine serum (A4766801; Gibco, ThermoFisher scientific, Waltham, USA) and a penicillin/streptomycin solution (5.000U: 15070063; Gibco, ThermoFisher scientific, Waltham, USA). Cultures were maintained in a humidified atmosphere with 5% CO_2 at 37°C. To synchronize the cell population prior to differentiation, the percentage of FBS was reduced to 1%, and the cells were incubated in this restricted medium for 48 hours. For differentiation into granulocyte-like cells, HL-60 cells were then incubated with 1.5% dimethyl sulfoxide (DMSO; D2650; Merck Life Sciences BV; Hoeilaart, Belgium) for 5 days. After the differentiation period, cell viability was assessed using the Eve™ plus cell automatic counter (NanoEnTek; Seoul, Korea).

For NETosis induction, differentiated cells were resuspended at a concentration of 10^6 cells/mL in IMDM without additives. The resuspended cells were then seeded in 6-well plates with 2 mL of cell suspension per well (2 x 10^6 cells/well). To induce NETosis, 100 nM phorbol 12-myristate 13-acetate (PMA; J63916; ThermoFisher scientific, Waltham, USA) or 4 µM calcium ionophore A23187 (CI, C7522, Merck Life Sciences BV; Hoeilaart, Belgium) was added to each well, except for control condition, and the cells were incubated for 5 hours (for PMA conditions) or 3 hours (for CI conditions). For control conditions, cells were incubated with an equivalent volume of DMSO, the PMA and CI diluent. After the incubation period, the cells adhering to the bottom of the wells were scraped and the entire contents of the wells were collected into Falcon conical tubes (430291; Corning Life Sciences; Corning, USA). The tubes were then centrifuged at 200 g for 2 minutes to remove cell debris. The supernatant, containing NETs extruded in the IMDM, was collected. Finally, to increase the stability of the samples during their storage at −80°C, 20% glycerol (G5516-100 mL; Merck Life Sciences BV; Hoeilaart, Belgium) was added into the tubes.

2.2. Human neutrophil isolation and NETosis induction

Human neutrophil isolation was performed within one hour of blood collection using the MACSxpress Whole Blood Neutrophil Isolation Kit (130-104-434; Miltenyi Biotec, Bergisch Gladbach, Germany) for humans as previously published [43]. At the end of this isolation step, the isolated neutrophils cell pellet was resuspended in prewarmed RPMI medium at 37°C at a concentration of 1–2 x 10^6 cells/mL for NETosis induction with 100 nM of PMA or 10 µM of CI.

2.3. Immunofluorescence microscopy

HL-60 cells were incubated in 6-well plates containing one coverslip (631−0150; VWR; Radnor, USA) coated with poly-L-lysine per well. During the NETosis induction period, cells adhered to the coverslips. Then, post-stimulation, samples

were fixed with 1.3% paraformaldehyde (047317.92; ThermoFisher scientific, Waltham, USA) for 30 minutes at room temperature (RT) and then blocked with 5% donkey serum (#D9663; Merck Life Sciences BV, Hoeilaart, Belgium) for 30 minutes at RT. The primary neutrophil cells were incubated at 37°C with 5% CO_2 for 3 hours, followed by fixation with 1% paraformaldehyde for 10 minutes before the immunostaining characterization. DNA was counterstained with 4',6-diamidino-2-phénylindole (DAPI; D1306; ThermoFisher scientific, Waltham, USA) and cell membranes with Cell Mask™ Orange (C10045; ThermoFisher scientific, Waltham, USA). The coverslips were incubated with primary antibodies directed against myeloperoxidase (MPO) (ab221847; Abcam, Cambridge, UK, dilution 1:100), histone H3.1 (Belgian Volition SRL, Isnes, Belgium, dilution 1:100), histone H3Cit (ab232939; Abcam; Cambridge, UK, dilution 1:50) or nucleosome (Belgian Volition SRL, Isnes, Belgium, dilution 1:50) for 2 hours at RT, protected from the light. This was followed by incubation with secondary antibodies conjugated with Alexa Fluor fluorochromes (dilution 1:1000) (Goat anti-rabbit IgG AF 647; A-21244; ThermoFisher scientific, Waltham, USA) (Goat anti-mouse IgG AF 488; A-11001; ThermoFisher scientific, Waltham, USA) (Donkey anti-mouse IgG AF 647; A-31571; ThermoFisher scientific, Waltham, USA) (Donkey anti-goat IgG AF 488; A-11055; ThermoFisher scientific, Waltham, USA) for 1 hour at RT, protected from the light. After staining, slides were mounted by adding one drop of Fluoromount-G mounting solution (00-4958-02; ThermoFisher scientific; Waltham, USA) on a glass slide and carefully placing a coverslip facing downwards on the medium. Mounted slides were dried overnight at RT, in the dark. NETs derived from differentiated HL-60 cells were visualized using a Zeiss LSM900 Airyscan confocal laser scanning microscope (Zeiss; Oberkochen, Germany) equipped with 63x and 40x magnification objectives. Images were acquired at the Morph-IM platform (UNamur Technology Platform for Morphology and Imaging). For experiments involving NETs generated by isolated primary neutrophils, imaging and analysis were performed using a Nikon AXR Confocal with NSPARC Super Resolution microscope (Nikon; Tokyo, Japan) at the Nikon Imaging Center at UC San Diego.

2.4. NETs immunoprecipitation

MyOne Tosylactivated magnetic beads (65501; ThermoFisher scientific; Waltham, USA) were coated with the following antibodies: an anti-histone H3.1 monoclonal antibody (Belgian Volition SRL, Isnes, Belgium) as previously described [44], an anti-nucleosome monoclonal antibody (Belgian Volition SRL, Isnes, Belgium), and an anti-MPO monoclonal antibody (475915; 3460549; Merck Life Sciences BV; Hoeilaart, Belgium). To immunoprecipitate proteins of interest, 500 µL of sample was incubated with 1 mg of coated beads for 1 hour at RT (for anti-H3.1- and anti-MPO-coated beads) or 37°C (for anti-nucleosome-coated beads) on a roller. Following the incubation, the beads retaining the precipitated proteins were pelleted using a magnetic separation rack and were washed three times on a roller. Then, the products of immunoprecipitation (IP) were assessed either by Western blotting for the protein profile or by Agilent 2100 Bioanalyzer (Agilent Technologies; Santa Clara, USA) for the DNA profile.

2.5. dsDNA extraction

Following the NETs IP protocol, DNA from both the supernatant post-IP and the immunoprecipitated material was extracted using QIAamp® DSP Circulating NA kit (61504; Qiagen; Venlo, The Netherlands) according to the manufacturer's instructions.

2.6. dsDNA size distribution

The extracted dsDNA from both the supernatant post-IP and the immunoprecipitated material were assessed using an Agilent 2100 Bioanalyzer with an Agilent High Sensitivity DNA Kit for fragment sizes of 50–7000 bp (5067; Agilent Technologies; Agilent Technologies; Santa Clara, USA), according to manufacturer's instructions.

2.7. Western blotting

Following the IP protocol, the complex of NETs bound to magnetic particles was incubated for 5 minutes at 95°C in Laemmli buffer (1610747; Bio-Rad, Hercules, USA) containing 10% of 2-mercaptoethanol (M6250; Merck Life Sciences BV;

Hoeilaart, Belgium). The magnetic beads were then pelleted on a magnetic separation rack and the supernatant containing the denaturated proteins was separated using acrylamide gels. 4–20% TGX precast gels (4561094; Bio-Rad, Hercules, USA) were used for electrophoresis under reducing conditions (Tris/Glycine/SDS; 1610772; Bio-Rad; Hercules, USA).

Proteins were transferred onto polyvinylidene difluoride (PVDF) membranes (1704272; Bio-Rad; Hercules, USA) using a semi-dry transfer system (Bio-Rad; Hercules, USA) for 7 minutes at up to 20V. The PVDF membranes were then blocked using Tris Buffer Saline (TBS) containing 1% casein (1706435; Bio-Rad; Hercules, USA) for 30 minutes to 1 hour before being incubated for 2 hours with anti-MPO (antibody recognizing the two subunits α and β of the protein MPO, 2 µg/mL; 475915; 3460549; Merck Life Sciences BV, Hoeilaart, Belgium), anti-histone H3 (0.5 µg/mL; 91297; 3162002; Active Motif, Carlsbad, USA), or anti-histone H4 antibody (1/1000; ab177840; Abcam; 1014591−13; Cambridge, UK) diluted in TBS containing 1% casein.

After the primary antibody incubation, the membrane was washed three times and then incubated with a detection reagent (VeriBlot antibody for IP Detection Reagent, ab131366; 1035165−4; Abcam, Cambridge, UK) for 1 hour at RT. Finally, after three additional washes, the membrane was incubated with SuperSignal™ West Dura Extended Duration Substrate (34076; ThermoFisher scientific; Waltham, USA) and the chemiluminescent signal was acquired using the Fusion-FX6 instrument and software (Vilber, Marne-la-Vallée, France). To reuse the same membrane for different stainings, each membrane was rinsed three times with TBS containing 0.1% of Tween®20 (T2700; Merck Life Sciences BV; Hoeilaart, Belgium) (TBS-T) and subjected to a mild stripping protocol. Briefly, the membrane was incubated with stripping buffer, composed of Glycine 0.2 M (17-1323-01; GE Healthcare Technologies, Chicago, USA); sodium dodecyl sulfate 0.1% (24730−020; ThermoFisher scientific, Waltham, USA) and Tween®20 1% (T2700; Merck Life Sciences BV, Hoeilaart, Belgium) at pH 2.2 (± 0.1) for 10 minutes twice, washed with PBS 1x for 10 minutes twice, and washed with TBS containing 0.1% of Tween®20 (TBS-T) for 5 minutes twice before being blocked again. The rest of the protocol remained the same as described previously in this section. The efficiency of stripping was checked by incubating the membrane with chemiluminescent detection reagent just before the second blocking step.

2.8. Quantification of nucleosomes with the Nu.Q® ChLIA assays

H3.1- and H3R8Cit-nucleosome levels were measured using the Nu.Q® H3.1 (2001-02-01; Belgian Volition SRL, Isnes, Belgium) and Nu.Q® H3Cit ChLIA assays (Belgian Volition SRL, Isnes, Belgium), respectively. Both assays were developed on the IDS-i10 automated chemiluminescence immunoanalyzer system (Immunodiagnostic Systems Ltd, Boldon, UK) with magnetic beads technology. Briefly, 50 µL of samples are mixed with an acridinium ester labeled anti-nucleosome detection antibody and incubated for 30 minutes. The conformational antibody ensures that the measured analyte is the nucleosome itself, distinguishing it from individual histones or circulating DNA. Anti-histone H3.1 or H3Cit antibody-coated magnetic beads were then added and incubated for an additional 15 minutes. Following incubation, a washing step was performed to remove unbound components. Trigger solutions were added, and the emitted light was recorded using the luminometer. A standard curve specific for each assay was used for calibration. Sample quantification was performed using a 4-parameter logistic curve fitting. The Nu.Q® H3.1 assay quantifies H3.1-nucleosome concentration from 3 to 1200 ng/mL. Samples exceeding 1200 ng/mL were automatically remeasured following an automated 5-fold dilution by the instrument, extending the quantification range up to 6000 ng/mL. The Nu.Q® H3Cit assay quantifies H3Cit-nucleosome concentration from 5 to 500 ng/mL.

2.9. Quantification of nucleosomes with the H3Cit-DNA and MPO-DNA ELISA assays

The H3Cit-DNA and MPO-DNA ELISA assays were performed according to previously published protocols. The H3Cit-DNA ELISA was carried out following the method described by Thålin et al. [30], which detects citrullinated histone H3 in complex with DNA. The MPO-DNA ELISA was conducted as described by Rada et al. [31], which quantifies complexes of myeloperoxidase bound to DNA as a surrogate marker of NETs.

2.10. Analytical performances evaluation of the H3.1-nucleosome ChLIA assay

Experimental designs for evaluating the analytical performances of the H3.1-nucleosome assay for K2EDTA plasma measurements followed the recommendations of the CLSI guidelines. Precision was assessed by measuring five samples with different concentration levels, obtained by spiking human K2EDTA plasma samples with native nucleosomes extracted from human cells. The samples were measured, using three lots of reagents over 7 days, with two runs per day and two measurements per run (3 x 7 x 2 x 2 design). Coefficients of variation percentages (CV%) were calculated based on CLSI-EP05A suggested analysis of variance using the Analyse-it software, allowing evaluation of repeatability, within-lot precision, and within-laboratory precision.

Sensitivity limits were determined based on CLSI guideline EP17-A2 suggestions, using three independent lots of reagents. For the limit of blank (LOB), 60 measurements of diluent were conducted over 5 days, and the LOB was calculated as the average value plus 1.645 standard deviation (SD), representing the 95th percentile of the normal distribution. The limit of detection (LOD) was calculated by measuring 10 human K2EDTA plasma samples, ranging from approximately 0–10 ng/mL, in triplicates over 5 days. The pooled standard deviation (pooled SD) for all the measurements was determined and the LOD was calculated as follows: *LOD = LOB + 1.645 pooled SD of non-blank samples*. Finally, the lower limit of quantification (LOQ) was defined for three lots of reagents using a precision profile, setting 15 CV% as the maximum limit of imprecision allowed for precise quantification.

For the evaluation of the linearity, human K2EDTA plasma samples of different concentrations were mixed in equivalent proportions (per 10% levels) and linear curve fitting with variance-based weighting were applied. The linear ranges were established by comparing measured concentrations of the different sample proportions with linear regression expected concentrations. The linearity range defines the range within which the difference between measurement and linear model predictions is less than 10%.

In spike-recovery experiments, three samples were spiked with two concentrations of recombinant nucleosomes and compared with these samples added with the same volume of diluent. The percentage of recovery was evaluated by normalizing the measured concentration of spiked samples with the expected nucleosome concentration (measured concentration of the control + spiked concentration).

Interferences were evaluated by comparing nucleosome concentrations in plasma samples with and without the addition of the following components: bilirubin (conjugated or unconjugated), human serum albumin, triglycerides, cholesterol, or hemoglobin at different concentrations (representing high, non-normal concentrations). For human anti-mouse antibodies and rheumatoid factors, a spike recovery was conducted in samples with known concentrations of these two heterophilic antibodies to verify the absence of false positive or false negative influence.

Cross-reactivity was tested by measuring single H3.1-histone and H3.3-containing nucleosomes, as well as citrullinated recombinant nucleosomes H3R8Cit and H3R2,8,17Cit.

Carryover was investigated by repeatedly measuring a sample of low and a sample of high nucleosome concentrations to ensure that the order of measurement did not influence the precision or accuracy of the measurements.

2.11. Studies' population

The comparative NET-assays study included K2EDTA plasma samples from healthy donors (n = 55), as well as patients with COVID-19 (n = 13) and sepsis (n = 31). The broader study included 236 samples from control donors, self-certified as healthy donors from EFS (Etablissement Français du Sang) and 302 samples from patients with diseases associated with NETosis such as COVID-19 (n = 80), sepsis suspicion and confirmed (n = 109), cirrhosis or nonalcoholic steatohepatitis (n = 11), cytomegalovirus infection (n = 23), gonorrhea infection (n = 10), myocardial infarction (n = 38), Alzheimer's disease (n = 12), hepatitis A virus infection, (n = 6), Lyme infection (n = 6), traumatic brain injury (n = 6), and heart failure (n = 1). Diagnoses were provided by the respective biobank suppliers.

Frozen K2EDTA plasma samples used were sourced from certified biobanks, including INOSpecimens, BioIVT, DxBioSamples, BayBiosciences, and QUALIblood and were received anonymized. All specimens were either collected from consented donors or provided as de-identified remnant samples. Each biobank adheres to stringent ethical policies and implements state-of-the-art procedures to ensure the highest ethical standards in its operations in accordance with the Declaration of Helsinki, ensuring the protection of human subjects. For samples obtained from INOSpecimens BioBank (Clermont Ferrand, France), the biobank holds authorization to commercialize residual samples from medical analyses for scientific research purposes (AC-2018–3151, AC-2022–4975). Samples from the other biobanks were retrospectively collected and made available for research in compliance with applicable national regulations. All enrolled patients signed specific informed consent forms for blood draw and related translational research projects. The protocol/study numbers for all the samples tested are as follows: BioIVT (Frankfurt, Germany) 2020–002/1282289; DxBioSamples LLC (San Diego, California, USA) PG-ONC 2003/1; BayBiosciences LLC (Brookline, Massachusetts, USA) BBS-TPP-817–22; QUALIblood (Liège, Belgium) B03920096633 49/2009.

The studies are research studies conducted on retrospective biobanked samples. They are not clinical trials and do not involve the recruitment of new participants. Therefore, ethical approval is not required for these studies.

2.12. Statistical analysis

Analytical data were analyzed using Analyse-it for Microsoft Excel (version 5.9) software. The linearity of the model was assessed through simple linear regression using linear fit model, allowing ±10% of non-linearity.

Descriptive statistical analysis of the clinical dataset was performed using GraphPad Prism (version 9.5.0, San Diego, CA, USA). The data were subjected to the Kolmogorov– Smirnov normality test. Group comparisons were conducted using Welch's test and the Mann–Whitney U test for non-parametric data. Specificity, sensitivity, negative predictive value, and positive predictive value were calculated. The area under the curve (AUC) were calculated from the receiver operator characteristic (ROC) curve. The Youden Index (J), defined as $J = Sensitivity + Specificity - 1$ was employed to identify the optimal threshold. Significance values are represented as follows: *, p-value (p) < 0.05; **, $p < 0.01$; ***, $p < 0.001$; ****, $p < 0.0001$.

3. Results

3.1. The molecular characterization of NETs produced *in vitro* confirms the presence of H3.1-nucleosomes

HL-60 promyeloblastic cells can be differentiated into neutrophil-like cells through exposure to dimethyl sulfoxide (DMSO). Once differentiated, subsequent treatment with phorbol 12-myristate 13-acetate (PMA) induces NETosis. Similarly, PMA triggers NETosis in primary human neutrophils isolated from whole blood. To confirm NETosis induction by PMA treatment, we compared the presence of NET structures in PMA-treated DMSO-differentiated HL-60 cells (DMSO-dHL-60 + PMA) with those in untreated cells (DMSO-dHL-60) (S1 Fig). In DMSO-dHL-60 cells, the fluorescent microscopy images showed intact cell membranes stained with Cell Mask™ Orange and intact nuclei marked with DAPI, indicating the absence − or a weak induction − of NETosis. In contrast, PMA-treated cells exhibited cell membrane debris and large extruded DNA filaments, confirming NETosis activation. Then, we analyzed, the putative spatial relationship between NETs and H3.1-nucleosomes in the two *in vitro* NETs models − the DMSO-dHL-60 + PMA model and the Primary Neutrophils +PMA model −, using antibodies directed against the protein MPO, the histone variant H3.1, the citrullinated histone H3 (H3Cit), and the nucleosome. The immunostaining revealed that DNA staining (DAPI), MPO, histone H3.1, histone H3Cit, and nucleosome signals colocalize in extruded NETs released from DMSO-dHL-60 + PMA cells (Fig 1A–D). Similarly, immunostaining on PMA-activated human neutrophils confirmed the colocalization of MPO, DNA, H3Cit and H3.1 within NETs (Fig 1E–F). Altogether, this colocalization indicates the close proximity of these components, suggesting they are part of the same structural entity.

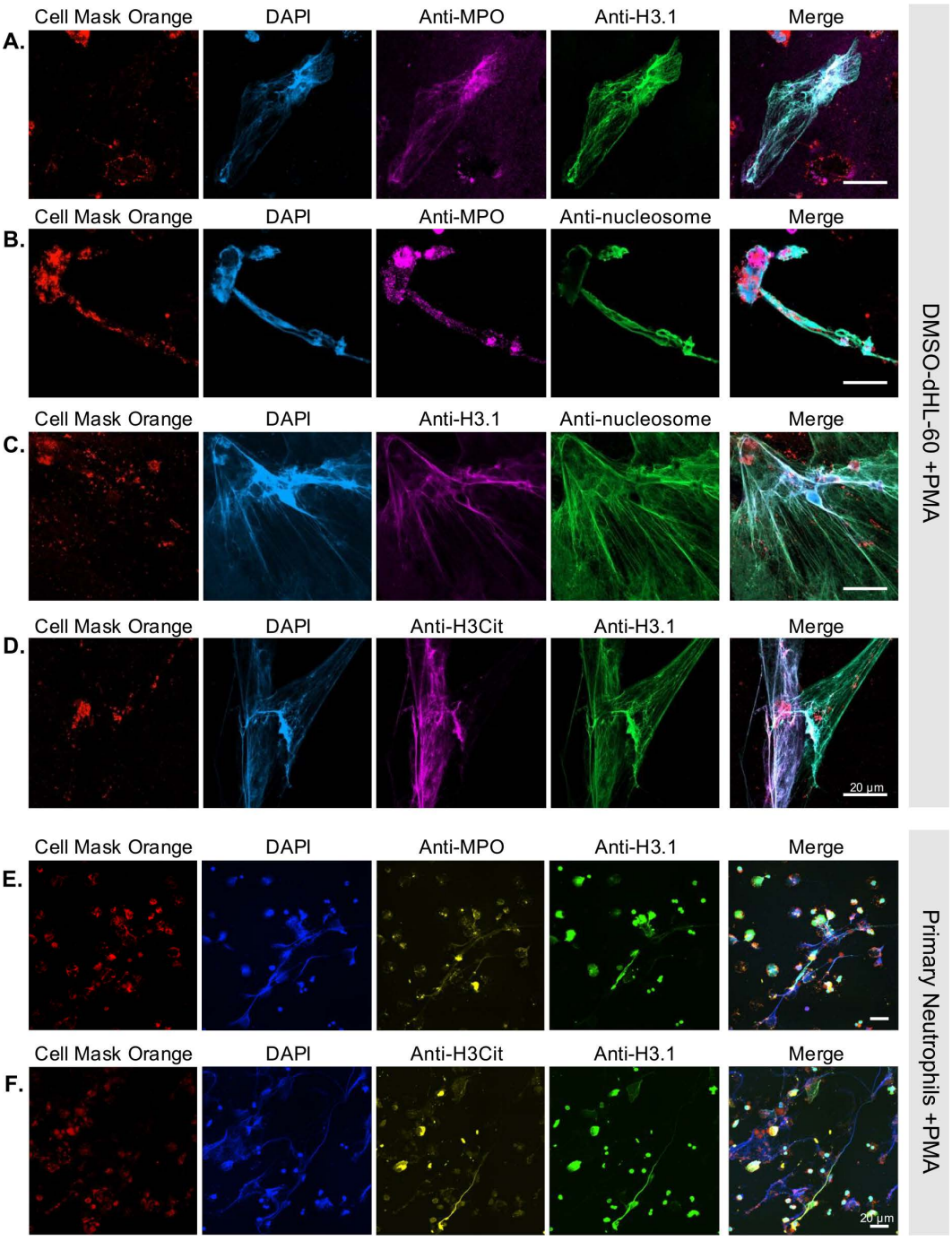

Fig 1. Immunostaining of NETs derived from HL-60 cells or primary neutrophils demonstrates the presence of H3.1-nucleosomes. Neutrophil-like DMSO-differentiated HL-60 cells (A-D) or primary neutrophils isolated from human whole blood (E-F) treated with PMA were stained with anti-MPO (A and B, purple; E, yellow), anti-histone H3.1 (A, D, E and F, green; C, purple), anti-nucleosome (B and C, green) or anti-H3Cit (D, purple; F, yellow) antibodies. DNA and membranes were stained with DAPI (blue) and Cell Mask™ Orange (orange-red), respectively. Scale bars, 20μm. DMSO, dimethyl sulfoxide; PMA, phorbol 12-myristate 13-acetate; MPO, myeloperoxidase; NETs, neutrophil extracellular traps.

https://doi.org/10.1371/journal.pone.0329352.g001

To confirm that H3.1-nucleosomes are released during NETosis triggered with inducers other than PMA, we also immunostained NETs derived from both DMSO-dHL-60 cells or primary neutrophils treated with calcium ionophore A23187 (CI). The results obtained show that H3.1-nucleosomes colocalize with DNA and MPO and support the conclusion that H3.1-nucleosomes are released during NETosis, irrespective of the NETosis inducer used (S2 Fig).

We further investigated, in the DMSO-dHL-60 NETs model, the interactions between MPO and H3.1-nucleosomes by immunoprecipitation (IP) followed by Western blots (Fig 2A). Characterization of the pulled-down proteins demonstrated that nucleosomes precipitated with either an anti-nucleosome antibody (IP anti-nucleosome) or an anti-H3.1 antibody (IP anti-H3.1) co-immunoprecipitated with the two subunits of MPO (MPOα and MPOβ), as well as histones H3 and H4. The different bands observed with the H3-antibody indicate the presence of various forms of histone H3, likely reflecting proteolytic cleavage events of this protein. Conversely, IP with anti-MPO-coated particles (IP anti-MPO) resulted in the co-IP of histones H3 and H4 as well as the two subunits of MPO (MPOα and MPOβ), suggesting that MPO and H3.1-nucleosomes interact closely in this NETs structure.

Furthermore, to confirm that the H3.1-nucleosomes immunoprecipitated were part of NETs, we investigated their DNA fragment size profiles using Agilent 2100 Bioanalyzer. The analysis revealed that the DNA fragments immunoprecipitated with anti-H3.1-, anti-nucleosomes-, and anti-MPO-coated beads measured thousands of base pairs consistent with the large NET filaments (Fig 2B–D). The DNA characterization of the material remaining in the supernatant after IP anti-H3.1 and IP anti-nucleosome (post-IP) showed an absence of DNA, confirming that these IPs effectively captured all NET structures. In contrast, the IP anti-MPO demonstrated only partial retention of the DNA, indicating incomplete capture of the NET structures in this condition. Control experiments performed with immunoglobulin (Ig) G2A and IgG rabbit isotypes magnetic particles did not significantly precipitate either MPO, histone H3, histone H4 (Fig 2A), or DNA (Fig 2E–F), confirming the specificity of the IPs.

Subsequently, to validate the interaction between the NET components and H3.1-nucleosomes, we quantified the depletion of H3.1-nucleosomes following IP anti-nucleosome, IP anti-H3.1, and IP anti-MPO. Quantification results revealed a 97% depletion of H3.1-nucleosomes after IP anti-nucleosome, 99% depletion after IP anti-H3.1, and 30% depletion after IP anti-MPO, confirming the partial co-IP of H3.1-nucleosomes and MPO (S1 Table). IP with IgG2a isotype and IgG rabbit isotype controls did not result in nucleosome depletion confirming the specificity of the IP.

Overall, our findings confirm interactions between H3.1- nucleosomes, MPO, and DNA, demonstrating the presence of H3.1-nucleosomes within NETs and highlighting the utility of H3.1-nucleosome quantification as a reliable marker for NETs detection.

3.2. Development of a ChLIA for quantification of H3.1-nucleosomes in plasma

We then developed and analytically validated an automated chemiluminescent magnetic bead-based immunoassay to measure H3.1-nucleosomes in K2EDTA plasma samples. This sandwich assay uses the anti-histone H3.1 antibody coated on magnetic particles and an anti-nucleosome conformational antibody in the liquid phase. The linear range for the assay was established between 26.3 ng/mL to 215.9 ng/mL (Mix 1, Fig 3A), 201.4 ng/mL to 971.8 ng/mL (Mix 2, Fig 3B), and 389.8 ng/mL to 1214.4 ng/mL (Mix 3, Fig 3C). Combining these results, the linear quantification range for the H3.1-nucleosome assay spans from 26.3 ng/ml to 1214.4 ng/mL (Fig 3D and S2 Table). This range was verified by fitting a linear model based on the three combined mixes (33 proportions; combined mixes, Fig 3D). Additionally, for samples with H3.1-nucleosome levels higher than 1200 ng/mL, we developed and validated an automatic 5-fold dilution to extend the range, resulting in a linear quantification range for the H3.1-nucleosome assay from 26.3 ng/mL to 6000 ng/mL. All limit of blank (LOB), limit of detection (LOD), and limit of quantification (LOQ) values estimated for three independent lots of reagents were below 3 ng/mL (mean ± standard deviation [SD]: LOB = 0.33 ± 0.06; LOD = 0.93 ± 0.06; LOQ = 2.30 ± 0.14), defined as the assay limit (Fig 3E).

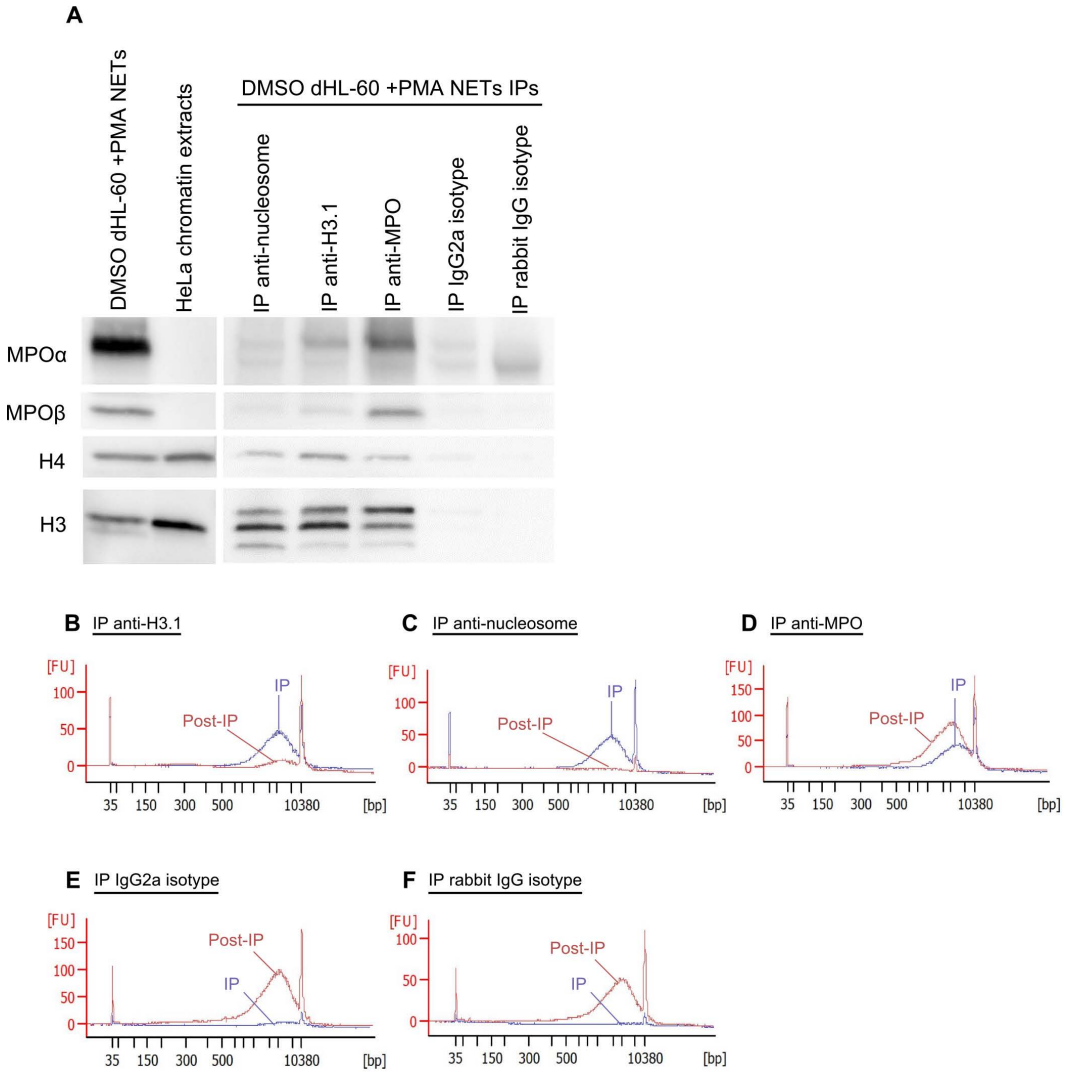

Fig 2. Molecular characterization of NETs from differentiated HL-60 cells demonstrates the presence of H3.1-nucleosomes. NET extracts from DMSO-differentiated HL-60 cells treated with PMA (DMSO-dHL-60 + PMA NETs) (A, lane 1), HeLa chromatin extracts (A, lane 2), and proteins pulled-down by using magnetic particles coated with anti-nucleosome (A, lane 3), anti-H3.1 (A, lane 4), anti-MPO (A, lane 5), IgG2a isotype (A, lane 6) and IgG rabbit isotype (A, lane 7) were analyzed using SDS-PAGE followed by anti-MPO, anti-H4 and anti-H3 Western blotting. The anti-MPO antibody detects both α and β sub-units of the MPO protein. The H3 antibody targets the C-terminal extremity of the histone H3. Cell-free DNA fragment size distribution of DNA immunoprecipitated (IP, blue) or left in the supernatant (post-IP, red) by anti-H3.1 (B), anti-nucleosome (C), anti-MPO (D), IgG2A isotype (E), and IgG rabbit isotype(F)-coated particles were analyzed using Agilent 2100 Bioanalyzer. DMSO, dimethyl sulfoxide; Ig, immunoglobulin; MPO, myeloperoxidase; NETs, neutrophil extracellular traps; PMA, phorbol 12-myristate 13-acetate; SDS-PAGE, sodium dodecyl-sulfate polyacrylamide gel electrophoresis.

https://doi.org/10.1371/journal.pone.0329352.g002

Then, the assay precision was assessed, and quantification was performed either by calibrating the assay daily (Table 1A) or using a single calibration per reagent lot on the first day (Table 1B). Within-run coefficients of variation (CV) ranged from 1.4% to 2.8%, within-lot CV from 2.9% to 6.4%, and within-laboratory CV from 3.1% to 9.2%, depending on the sample considered. Interestingly, while bias in concentration between daily and single calibration was limited, single calibration induced slightly higher imprecision, though still reasonable.

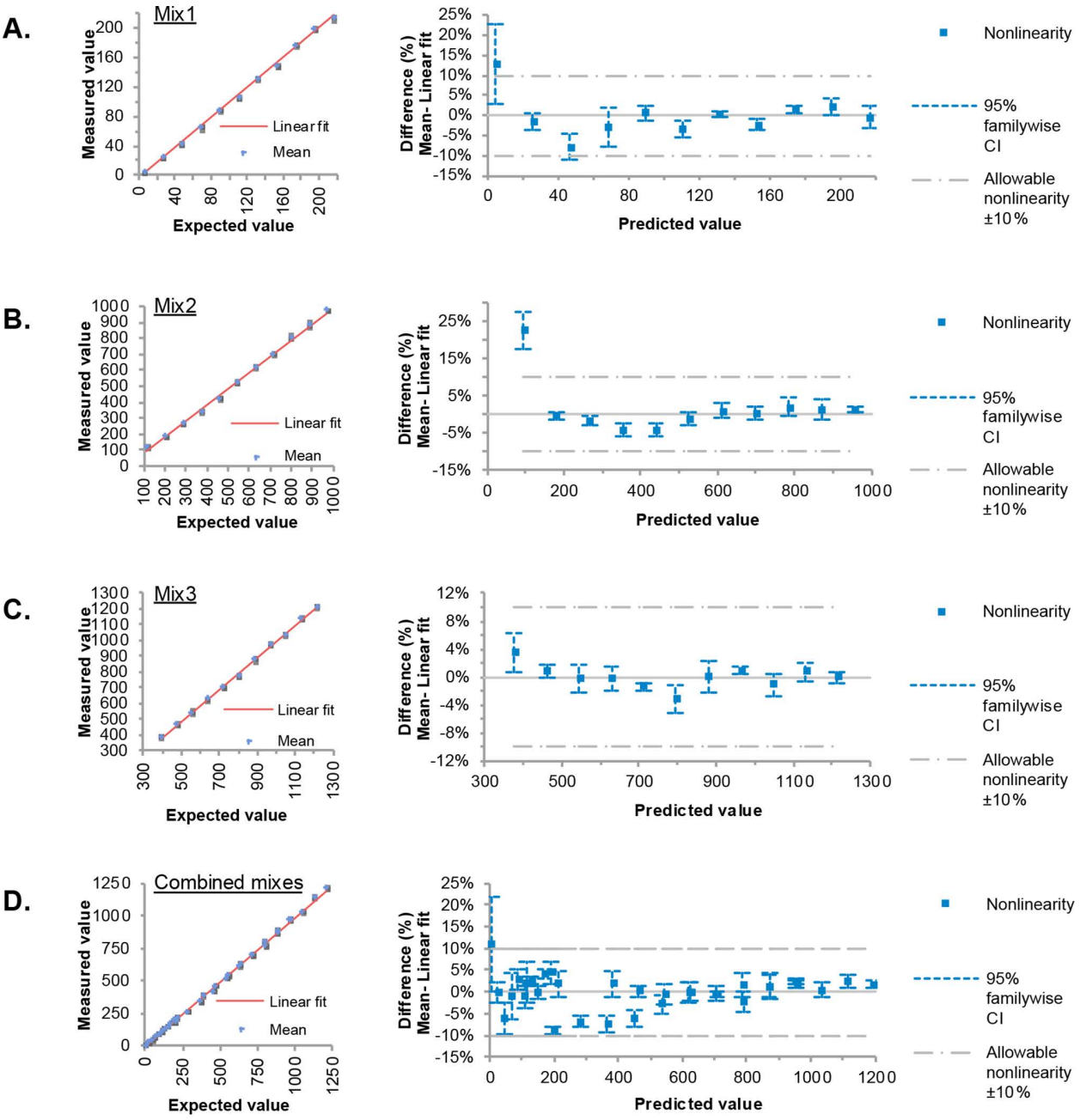

E.

	LOT 1	LOT 2	LOT 3
LOB	0.4 ng/mL	0.3 ng/mL	0.3 ng/mL
LOD	1.0 ng/mL	0.9 ng/mL	0.9 ng/mL
LOQ	2.2 ng/mL	2.4 ng/mL	1.7 ng/mL

Fig 3. H3.1-nucleosome immunoassay linearity and sensitivity. Three K2EDTA plasma samples containing low concentrations of H3.1-nucleosomes were each mixed into three other K2EDTA plasma samples of higher H3.1 concentrations [(A) Mix 1, (B) Mix 2 or (C) Mix 3] to prepare 11 proportions and measured with the H3.1-nucleosomes immunoassay. Scatter plots show the linearity of the measurement, expressed in ng/mL, over the measuring intervals (expected value). The red line shows the linear fit. The linearity plots show the difference between the linear and nonlinear fit across the

measuring interval. (D) Combined results from Mixes 1–3. (E) H3.1-nucleosomes assay limits of blank (LOB), limits of detection (LOB) and limits of quantification (LOQ) estimated for three independent lots of reagents. CI, confidence.

https://doi.org/10.1371/journal.pone.0329352.g003

Five samples with increasing H3.1-nucleosome concentrations were measured using three lots of reagents, for seven days with two runs per day and two measurements per run (3 lots x 7 days x 2 runs x 2 measurements = 84 measures/sample). Quantifications were done using a daily calibration for each lot (A) or using a unique standard curve/lot at day 1 (B). A nested analysis was conducted to evaluate repeatability, within-lot and within-laboratory standard deviation (SD) and coefficients of variation (CV) for each sample. Bias of quantification was calculated to compare daily and single calibration. Levels 2–5 were prepared by spiking K2EDTA samples with cell-line extracted nucleosomes.NETs, neutrophil extracellular traps.

Additionally, a spike-recovery study was performed by adding known concentrations of H3.1-nucleosome into three independent K2EDTA plasma samples. Recovery rates ranged from 89% to 105%, indicating no matrix effect (Table 2).

Three independent K2EDTA plasma samples were quantified with the H3.1-nucleosome immunoassay before and after the addition of 93.5 or 187.0 ng/mL of H3.1 recombinant nucleosome. The quantifications are expressed in ng/mL. The percentage of recovery was calculated by dividing the measured concentration (M) with the expected concentration (E).

Then, the specificity of the H3.1-nucleosome ChLIA assay for the H3.1-nucleosome structure was confirmed by testing the recombinant H3.3-nucleosome and the recombinant H3.1-histone, both exhibiting a cross-reactivity lower than 2%. Interestingly, when recombinant H3.1-nucleosomes presenting citrullinated marks (H3R8Cit and H3R2, 8,17Cit) were tested in the assay, the quantification yielded values of 88.5% and 113.8%, respectively, relative to H3.1-nucleosomes (S3 Fig). These results demonstrate that the presence of citrulline marks on histone H3 does not interfere with the accurate quantification of H3.1-nucleosomes. Afterwards, common endogenous interference substances from plasma were tested by comparing H3.1-nucleosome measurements with and without these substances in plasma samples. S3 Table shows concentrations of these substances that impact H3.1-nucleosome measurements less than 10%.

Overall, these analytical validation results confirm that the H3.1-nucleosome ChLIA assay is precise, sensitive, specific, and robust for measuring H3.1-nucleosome concentrations in K2EDTA plasma samples.

Table 1. H3.1-nucleosome immunoassay precision.

A.	Daily calibration								
	SAMPLE	n	Mean concentration (ng/mL)	Repeatability CV	Repeatability SD	Within Lot CV	Within Lot SD	Within-laboratory CV	Within-laboratory SD
	Level 1	84	14.7	2.80%	0.4	5.80%	0.8	7.10%	1
	Level 2	84	52.2	1.90%	1	3.50%	1.8	7.10%	3.7
	Level 3	84	208.6	1.40%	2.9	3.50%	7.2	5.00%	10.5
	Level 4	84	439.6	1.50%	6.6	2.90%	12.7	3.10%	13.5
	Level 5	84	727.8	2.00%	14.9	3.50%	25.6	3.80%	27.3
B.	Single calibration Day 1								
	SAMPLE	n	Mean concentration (ng/mL)	Repeatability CV	Repeatability SD	Within Lot CV	Within Lot SD	Within-laboratory CV	Within-laboratory SD
	Level 1	84	15.2	2.70%	0.4	6.40%	1	7.40%	1.1
	Level 2	84	53.2	1.80%	1	5.20%	2.7	6.30%	3.3
	Level 3	84	210.1	1.40%	2.9	4.90%	10.3	7.00%	14.7
	Level 4	84	442.8	1.50%	6.6	4.60%	20.6	8.60%	37.9
	Level 5	84	735.9	2.20%	16.5	5.30%	38.9	9.20%	67.7

https://doi.org/10.1371/journal.pone.0329352.t001

Table 2. H3.1-nucleosome immunoassay spike recovery.

	Concentration (ng/mL)	Nucleosome added (ng/mL)	Measured (M) (ng/mL)	Expected (E) (ng/mL)	%Recovery (M/E)
Sample 1	190.0	93.5	269.7	283.5	**95%**
		187.0	366.3	377.0	**97%**
Sample 2	73.0	93.5	162.4	166.5	**98%**
		187.0	271.9	260.0	**105%**
Sample 3	112.3	93.5	183.7	205.8	**89%**
		187.0	297.9	299.3	**100%**

https://doi.org/10.1371/journal.pone.0329352.t002

3.3. The H3.1-nucleosome assay effectively detects NETs-related nucleosomes

Prior to investigating the clinical relevance of the H3.1-nucleosome ChLIA assay, we assessed its efficacy in detecting NETs-related H3.1-nucleosomes in PMA-treated DMSO-differentiated HL-60 cells. The assay showed a significant increase of H3.1-nucleosome levels in DMSO-differentiated HL-60 + PMA cells (here referred to as NETs; mean ± SD: 1306 ± 238 ng/mL) compared with the untreated DMSO-differentiated HL-60 cells (here referred to as controls; mean ± SD: 302 ± 175 ng/mL; ** $p = 0.0054$) (Fig 4A). In parallel, this assay's performance was compared with other potential NETs biomarkers such as the extracellular double-stranded DNA (dsDNA), the MPO-DNA complex measured using a widely referenced custom ELISA assay [31] and an in-house developed chemiluminescent immunoassay targeting H3Cit-nucleosomes (H3Cit-nucleosome ChLIA assay). While the H3Cit-nucleosome assay differentiated between PMA-treated (mean ± SD: 454 ± 138 ng/mL) and untreated DMSO-differentiated HL-60 (mean ± SD: 134 ± 103 ng/mL), its significance was lower; (* $p = 0.0364$) than that of H3.1-nucleosomes (Fig 4B). Extracellular dsDNA concentrations were significantly higher in PMA-treated DMSO-differentiated HL-60 cells (mean ± SD: 10.15 ± 0.57 ng/μL) compared to untreated cells (mean ± SD: 2.97 ± 0.92 ng/μL; *** $p = 0.0008$) (Fig 4C). Although MPO-DNA complex signal (optical density [OD]) was elevated in PMA-treated DMSO-differentiated HL-60 extracts (mean OD value 1.42 ± 0.69) compared with the control conditions (mean OD value 0.51 ± 0.07; $p = 0.1418$), the difference was not statistically significant (Fig 4D). Our findings confirm that the H3.1-nucleosomes ChLIA assay effectively detects H3.1-nucleosomes associated with NETosis in *in-vitro* model.

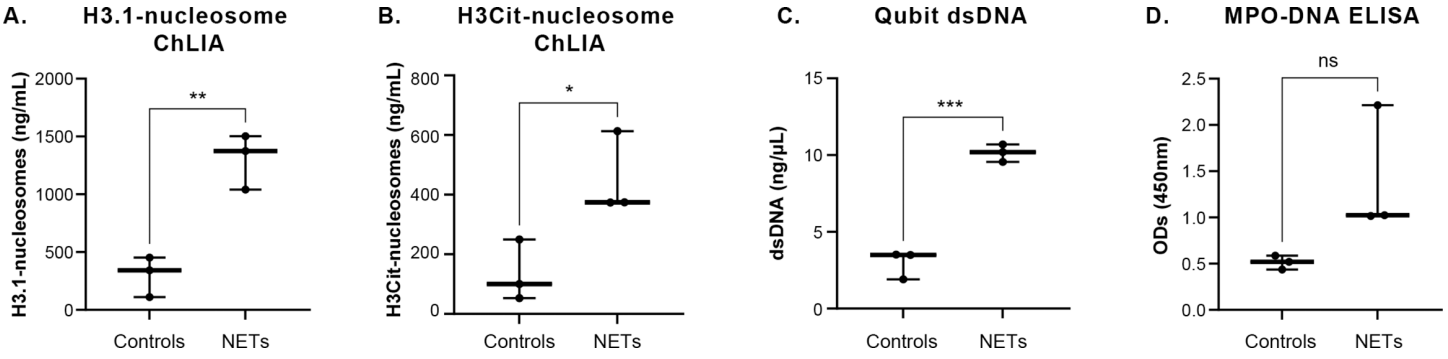

Fig 4. Comparative measures of H3.1-nucleosomes, H3R8Cit-nucleosomes, dsDNA and MPO-DNA complexes in NETs derived from HL-60 cells. Jitter plot analysis representation of the H3.1-nucleosomes (A), the H3Cit-nucleosomes (B), the dsDNA (C), and the MPO-DNA (D) measured for three independent productions of NET extracts (n = 3) from DMSO-differentiated HL-60 cells treated with PMA (NETs) compared with the untreated cells (Controls). ns represent non-significant p-value, *, ** and *** represent p-values <0.05, < 0.01 and <0.001, respectively, calculated using the Welch's test. Cit, citrullinated histone H3; dsDNA, double-stranded DNA; MPO, myeloperoxidase; NETs, neutrophil extracellular traps; OD, optical density.

https://doi.org/10.1371/journal.pone.0329352.g004

3.4. The H3.1-nucleosomes assay significantly distinguishes NETs-associated diseases from healthy controls

To study the clinical relevance of the H3.1-nucleosomes ChLIA assay, we first compared its performance with three other NETs-related assays. These included the in-house developed H3Cit-nucleosome chemiluminescent immunoassay, as well as two established ELISA assays: the H3Cit-DNA assay and the MPO-DNA assay. These assays were applied to a cohort of clinical samples composed of healthy donors (here refer as control, n = 55) and patients with NETs-associated diseases (here refer as NETs: sepsis; n = 31 and COVID-19; n = 13). While signal intensity and dynamic range varied across platforms, all four assays demonstrated a significant ability to distinguish NETs patients from healthy controls, as shown in Supplementary Fig 4 (S4 Fig, Panels A–D). ROC curve analyses confirmed their diagnostic value, with the H3.1-nucleosome assay achieving the highest area under the curve (AUC = 0.97), compared to the H3Cit-nucleosome assay (AUC = 0.77), MPO-DNA ELISA (AUC = 0.95), and H3Cit-DNA ELISA (AUC = 0.77) (S4 Fig, Panels E–H). These results demonstrate that while all tested assays are effective for NETs detection, the H3.1-nucleosome assay offers superior diagnostic performance and may represent a clinically applicable biomarker for detecting NETs-related conditions.

Then, we conducted a broader study using only the H3.1-nucleosome assay on a retrospective cohort (n = 538 patients) constituted by 302 K2EDTA plasma samples from patients presenting 11 different NETs-related pathologies and 236 K2EDTA plasma samples from healthy donors (n = 236 donors). The results indicated significantly elevated levels of circulating H3.1-nucleosomes in patients with NETs-related pathologies (here referred to as NETs patients) compared with the control population (here referred to as Healthy donors – mean 721.00 ng/mL vs 30.66 ng/mL, **** $p < 0.0001$) (Fig 5A). Furthermore, to evaluate the performance of the assay in distinguishing patients suffering from NETs-related diseases vs heathy individuals, we generated a receiver-operating characteristic (ROC) curve. The area under the ROC curve (AUC) was calculated as 0.91 (95% CI: 0.89–0.94) (Fig 5B and S4 table). A sensitivity of 85.8% at 86.9% of specificity was observed at the optimal threshold of 47.25 ng/mL, as defined using the Youden Index. The positive predictive value and the negative predictive value were 89.31% and 82.66%, respectively. The results of this study confirmed the clinical efficacy of the H3.1-nucleosomes ChLIA assay in detecting elevated levels of circulating nucleosomes in patients with NETs-related pathologies. The high sensitivity and specificity, combined with robust predictive values, highlight the potential of this assay for clinical use in identifying NETs-related conditions.

4. Discussion

During NETosis, neutrophils release their decondensed DNA associated with histones and host defense proteins such as MPO and NE into the extracellular space to trap pathogens [9,45]. However, excessive NETs formation or impaired clearance can have detrimental effects and has been described in various pathologies including sepsis, COVID-19, rheumatoid arthritis, systemic lupus erythematosus, and others. This highlights the clinical relevance of monitoring NETs in blood samples. Given the central role of NETs in these diseases, their quantification could serve as a biomarker and/or risk factor for disease severity, potentially aiding personalized treatment strategies.

Despite growing interest in NETs, the absence of standardized, quantitative, and high-throughput methods for their detection remains a major limitation, underscoring the need for consistent methodologies. Most current approaches for NETs quantification rely on immunostaining and imaging-based techniques [46–50], which, while effective for visualizing NET structures, are time-consuming, semi-quantitative, and not easily scalable for high-throughput clinical use particularly for liquid biopsy applications [51]. Automated fluorescence microscopy-based methods [52] can mitigate some of these limitations but remain complex and resource-intensive. ELISA-based assays targeting NET components such as MPO, citrullinated histone H3, or DNA are also widely used to detect NETs [29,32,45,53,54]. Although informative, these assays are often semi-quantitative, with results expressed in absorbance or relative fluorescence units [32], or calibrated using “in-house” standards [30], limiting cross-laboratory and inter-study comparisons. Moreover, they typically detect

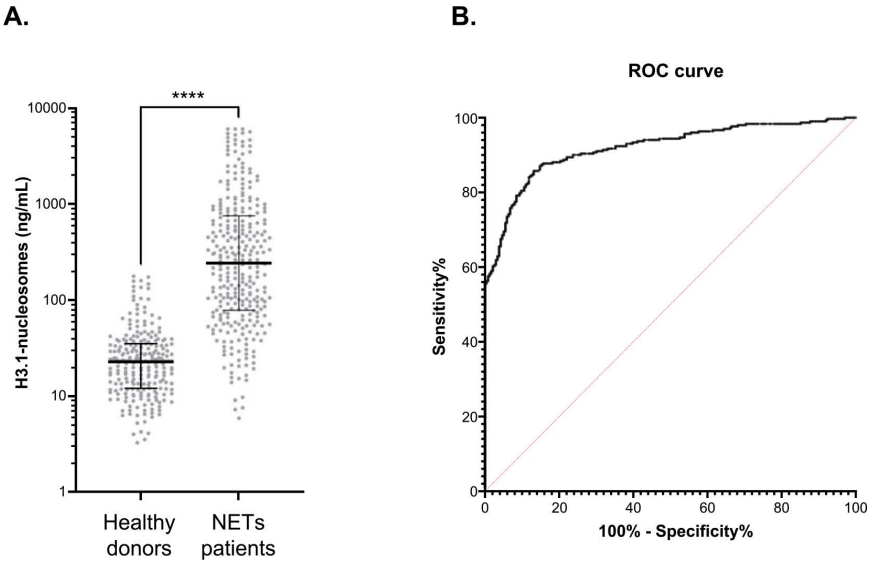

Fig 5. The H3.1-nucleosome assay significantly distinguishes NETs-associated diseases from healthy controls. (A) Jitter plot analysis representation of the circulating H3.1-nucleosomes level (ng/mL). The whiskers represent the 25th–75th percentile with median. **** represent p-value <0.0001, calculated using the Mann–Whitney U test. (B) ROC curve analysis of circulating H3.1-nucleosomes for discrimination of NETs patient's vs control samples. The area under the curve is 0.91 (95% CI: 0.89–0.94; $p < 0.0001$). CI, confidence interval; NETs, neutrophil extracellular traps; ROC, receiver operating characteristic.

https://doi.org/10.1371/journal.pone.0329352.g005

only a subset of NETs-associated structures, and their performance can vary depending on the specific NETosis pathway involved.

A major challenge in NETs quantification is indeed the biological heterogeneity of NETosis itself. It is now well accepted that NETosis can proceed through multiple mechanisms. Two main pathways have been described: the NADPH-oxidase dependent, triggered by PMA, certain bacteria, or pro-inflammatory cytokines, and involving the PKC signaling cascade, MPO and NE; and the NADPH-independent pathway, induced by calcium ionophores and characterized by peptidyl arginine deiminase 4 (PAD4) activation and histone H3 citrullination, a widely recognized NET biomarker [55–57]. However, PAD4-independent NETosis pathways lacking H3Cit have been reported [58–60], suggesting that H3Cit may not be a reliable marker in all NET contexts. Likewise, MPO −although broadly used in NETs assays− is not a universal marker; it is required for PMA-induced NETs but dispensable in NETs triggered by bacterial stimuli [58], and it can be released during degranulation independently of NET formation [61], reducing its specificity. Together, these findings suggest that H3Cit and MPO may not universally detect all NETosis events.

To address these limitations, we investigated the presence and relevance of H3.1-nucleosomes as NETs-associated markers. Using both the HL-60 *in vitro* model [41,42] and primary human neutrophils [43], treated with PMA or CI to induce NETosis, we confirmed the presence of H3.1-nucleosomes within NETs. Immunostaining experiments revealed colocalization of histones H3.1 and H3Cit with DNA and MPO, suggesting a close interaction among these components as well with nucleosomes, indicating that H3.1-nucleosomes are part of the NETs structure. Molecular characterization by co-immunoprecipitation further supported these findings, identifying complexes containing MPO, histones H3 and H4, and DNA. The consistency of these results across both the HL-60-derived model and primary neutrophils activated with PMA or Calcium ionophore, reinforces the robustness of H3.1-nucleosomes as NET-associated markers.

To build on these findings, we developed a chemiluminescent immunoassay to detect and quantify circulating H3.1-nucleosomes. The assay is automated, analytically validated according to Clinical & Laboratory Standards Institute

(CLSI) guidelines, and requires only 50 µL of K2EDTA plasma. It includes an internal calibrant to ensure consistency and comparability across laboratories. Chemiluminescence was selected over fluorescence detection due to its high sensitivity and its compatibility with automation, which reduces operator-dependent variability and facilitates routine use in diagnostic laboratories.

The H3.1-nucleosome assay is capable of detecting H3.1-nucleosomes regardless of post-translational modifications on histone H3 tails, including methylation, acetylation, phosphorylation, citrullination [62], or N-terminal tail cleavage. Indeed, during NETosis, neutrophil proteases can cleave the histone H3 N-terminal tail, potentially eliminating citrullinated epitopes and rendering some NET markers undetectable [63]. Supporting this, Western blot analysis using an antibody targeting the C-terminal region of histone H3 revealed multiple bands in PMA-treated DMSO-differentiated HL-60 cells, consistent with N-terminal cleavages of histone H3. Importantly, the H3.1-nucleosome assay is able to detect all these cleaved and modified forms of H3.1, enabling broad detection of nucleosomes. It is essential to admit that circulating H3.1-nucleosomes are not exclusive to NETosis and may arise from other forms of cell death, such as apoptosis or necrosis, and from cell types other than neutrophils. However, the markedly elevated H3.1-nucleosome levels observed in NETs-related diseases, compared to healthy controls or patients with diseases not primarily driven by NETs (e.g., cancers without significant systemic inflammation) underscores the relevance of the H3.1-nucleosome assay as an indicator of NETosis [64].

Based on this evidence, we evaluated the detection of H3.1-nucleosome by an immunoassay as a potential breakthrough method for objective, robust, reproductible and quantitative NETs detection. In PMA-treated DMSO-differentiated HL-60 cells, the assay detected elevated H3.1-nucleosome levels that correlated with established NETs markers, such as MPO-DNA, H3Cit-nucleosome and extracellular dsDNA. Similar results were also obtained in whole blood NETosis models [65], further validating the H3.1-nucleosome assay as a reliable indicator of NETosis.

Furthermore, we compared H3.1-nucleosome assay with other established NETs markers, including MPO-DNA (31), H3Cit-DNA [66], and H3Cit-nucleosome assay (in-house chemiluminescent assay), in a set of clinical samples. While signal intensity and dynamic range varied across methods, all four assays successfully distinguished NETs-related pathologies from controls. Notably, the H3.1-nucleosome assay demonstrated the highest diagnostic performance and the greatest clinical applicability, highlighting the potential of the H3.1-nucleosome immunoassay as a strong marker for NETs detection in liquid biopsy.

Finally, by measuring H3.1-nucleosome levels on a larger clinical cohort composed of K2EDTA plasma samples from both healthy donors and patients suffering from NETs-related diseases, we detected basal levels of H3.1-nucleosomes in healthy donors, reflecting the basal nucleosome release from dying and stressed cells into the blood circulation [4], while significantly elevated levels were detected in patients with NETs-related diseases, demonstrating the potential clinical utility of the H3.1-nucleosome assay as a robust tool for NETs detection. Further clinical studies will be required to validate H3.1-nucleosome measurements for risk prediction and prognosis in NETs-related diseases such as sepsis.

Supporting information

S1 Fig. PMA treatment induces NETs formation in DMSO-differentiated HL-60 cells. Neutrophil-like DMSO-differentiated HL-60 cells were treated during 5 hours with the NETosis-inducer PMA (PMA, lower panel), or not treated (DMSO, upper panel). DNA and membranes were stained with DAPI (Blue) and Cell Mask Orange (Orange-Red), respectively. Scale bars 50 µm.
(PDF)

S2 Fig. Immunostaining of NETs derived from HL-60 cells or primary neutrophils treated with calcium ionophore A23187 demonstrates the presence of H3.1-nucleosomes. Neutrophil-like DMSO-differentiated HL-60 cells (A-B) or primary neutrophils isolated from human whole blood (C-D) treated with Calcium Ionophore A23187 were stained with

anti-MPO (A and B, purple; C, yellow), anti-histone H3.1 (A, C and D, green), anti-nucleosome (B, green) or anti-H3Cit (D, yellow) antibodies. DNA and membranes were stained with DAPI (blue) and Cell MaskTM Orange (orange-red), respectively. Scale bars, 20μm.DMSO, dimethyl sulfoxide; CI, calcium ionophore A23187; MPO, myeloperoxidase; NETs, neutrophil extracellular traps.
(PDF)

S3 Fig. Detection of citrullinated H3.1-nucleosomes using the H3.1-nucleosome immunoassay. Quantification of H3.1-, H3R8Cit-, and H3R2,8,17Cit-recombinant nucleosomes using the H3.1-nucleosome immunoassay. Results are expressed as a percentage relative to the theoretical concentration of nucleosomes loaded in the samples (% recovery).
(PDF)

S4 Fig. Comparative measures of H3.1-nucleosomes, H3Cit-nucleosomes, MPO-DNA, and H3Cit-DNA complexes in plasma from control individuals and patients with NETs-related pathologies. Panels A to D present box plot analysis of H3.1-nucleosome levels (A; ng/mL), H3Cit-nucleosome levels (B; ng/mL), MPO-DNA complex levels (C; ODs), H3Cit-DNA complex levels (D, ng/mL) in control patients and in patients suffering of NETs-related diseases (Sepsis and COVID-19). The whiskers represent the 25th–75th percentile with median. **** represent p-value <0.0001, calculated using the Mann–Whitney U test. Panels E to H present ROC curve analysis of circulating H3.1-nucleosomes (E), H3Cit-nucleosomes (F), MPO-DNA complexes (G) and H3Cit-DNA complexes (H) for discrimination of control versus NETs samples. AUC, area under the curve.
(PDF)

S1 Table. H3.1-nucleosomes depletion after immunoprecipitation. H3.1-nucleosomes levels, expressed in ng/mL, indicate the depletion of nucleosomes after immunoprecipitation (IP) in comparison to the level present in the initial samples (HL-60 NETs unprocessed). Depletion results are expressed in %.NETs, neutrophil extracellular traps.
(PDF)

S2 Table. H3.1-nucleosome immunoassay linearity. NETs, neutrophil extracellular traps; Mean cc, mean of H3.1-nucleosomes assay concentration expressed in ng/mL.
(PDF)

S3 Table. H3.1-nucleosome immunoassay interferences and cross-reactivity. NETs, neutrophil extracellular traps.
(PDF)

S4 Table. Descriptive statistics. NETs, neutrophil extracellular traps; ROC, receiver operating characteristic.
(PDF)

S1 Raw Images. Original images supporting Western blot results reported in the main Figure 2A.
(PDF)

Acknowledgments

We acknowledge Marie Lurkin for her assistance in the processing of samples using the immunoassay automated platform and the Logistics team of Belgian Volition for their support. We thank Terry Kelly for her careful proofreading of the manuscript. We also thank the MorphIM Platform at the University of Namur for their expert guidance and assistance in generating and analyzing fluorescent microscopy images. Microscopy and image analysis of primary neutrophils was performed at the Nikon Imaging Center at UC San Diego. We'd like to thank Richard Sanchez and the Nikon Imaging Center at UCSD for the support on microscopy experiments.

Author contributions

Conceptualization: Marion Wargnies, Priscilla Van den Ackerveken, Marielle Herzog.

Formal analysis: Guillaume Rommelaere, Julie Candiracci, Dorian Pamart.

Investigation: Marion Wargnies, Guillaume Rommelaere, Robin Varsebroucq, Florian Jibassia, Finley Serneo, Virginie Laloux, Olivia Thiry, Fanny Lambert, Alison Lobbens, Priscilla Van den Ackerveken.

Methodology: Marion Wargnies, Guillaume Rommelaere, Julie Candiracci, Dorian Pamart, Priscilla Van den Ackerveken, Marielle Herzog.

Project administration: Marion Wargnies, Guillaume Rommelaere, Marielle Herzog.

Validation: Guillaume Rommelaere, Julie Candiracci, Dorian Pamart, Robin Varsebroucq, Florian Jibassia, Marielle Herzog.

Visualization: Marion Wargnies, Guillaume Rommelaere, Julie Candiracci, Alison Lobbens.

Writing – original draft: Marion Wargnies, Guillaume Rommelaere, Julie Candiracci, Dorian Pamart, Priscilla Van den Ackerveken.

Writing – review & editing: Marion Wargnies, Guillaume Rommelaere, Julie Candiracci, Dorian Pamart, Robin Varsebroucq, Florian Jibassia, Finley Serneo, Virginie Laloux, Olivia Thiry, Fanny Lambert, Alison Lobbens, Priscilla Van den Ackerveken, Marielle Herzog.

References

1. Cutter AR, Hayes JJ. A brief review of nucleosome structure. FEBS Lett. 2015;589(20 Pt A):2914–22. https://doi.org/10.1016/j.febslet.2015.05.016 PMID: 25980611
2. Clausell J, Happel N, Hale TK, Doenecke D, Beato M. Histone H1 subtypes differentially modulate chromatin condensation without preventing ATP-dependent remodeling by SWI/SNF or NURF. PLoS One. 2009;4(10):e0007243. https://doi.org/10.1371/journal.pone.0007243 PMID: 19794910
3. Kujirai T, Ehara H, Sekine SI, Kurumizaka H. Structural Transition of the Nucleosome during Transcription Elongation. Cells. 2023;12(10):1388. https://doi.org/10.3390/cells12101388 PMID: 37408222.
4. Holdenrieder S, Stieber P. Clinical use of circulating nucleosomes. Critical Reviews in Clinical Laboratory Sciences. 2009;46(1):1–24. https://doi.org/10.1080/10408360802485875 PMID: 19107649
5. Oliveri M, Daga A, Cantoni C, Lunardi C, Millo R, Puccetti A. DNase I mediates internucleosomal DNA degradation in human cells undergoing drug-induced apoptosis. Eur J Immunol. 2001;31(3):743–51. https://doi.org/10.1002/1521-4141(200103)31:3<743::aid-immu743>3.0.co;2-9
6. Rahier JF, Druez A, Faugeras L, Martinet JP, Géhénot M, Josseaux E, et al. Circulating nucleosomes as new blood-based biomarkers for detection of colorectal cancer. Clinical Epigenetics. 2017;9(1):53. https://doi.org/10.1186/s13148-017-0351-5 PMID: 28515797
7. Schulz C, Massberg S. Inflammaging aggravates stroke pathology. Nature Immunology. 2023;24(6):887–8. https://doi.org/10.1038/s41590-023-01516-y PMID: 37188943
8. Fuchs TA, Abed U, Goosmann C, Hurwitz R, Schulze I, Wahn V, et al. Novel cell death program leads to neutrophil extracellular traps. The Journal of Cell Biology. 2007;176(2):231–41. https://doi.org/10.1083/jcb.200606027 PMID: 17210947
9. Brinkmann V, Reichard U, Goosmann C, Fauler B, Uhlemann Y, Weiss DS, et al. Neutrophil Extracellular Traps Kill Bacteria. Science. 2004;303(5663):1532–5. https://doi.org/10.1126/science.1092385 PMID: 15001782
10. Burgener SS, Schroder K. Neutrophil Extracellular Traps in Host Defense. Cold Spring Harbor Perspectives in Biology. 2020;12(7):a037028-a.
11. Kaplan MJ, Radic M. Neutrophil extracellular traps: double-edged swords of innate immunity. The Journal of Immunology. 2012;189(6):2689–95. https://doi.org/10.4049/jimmunol.1201719 PMID: 22956760
12. Jorch SK, Kubes P. An emerging role for neutrophil extracellular traps in noninfectious disease. Nature Medicine. 2017;23(3):279–87.
13. Sørensen OE, Borregaard N. Neutrophil extracellular traps - The dark side of neutrophils. Journal of Clinical Investigation. 2016;1612–20. https://doi.org/10.1172/JCI84538 PMID: 27135878
14. Singh J, Boettcher M, Dölling M, Heuer A, Hohberger B, Leppkes M. Moonlighting chromatin: when DNA escapes nuclear control. Cell Death and Differentiation. 2023:861–75. https://doi.org/10.1038/s41418-023-01124-1 PMID: 36755071
15. Apel F, Zychlinsky A, Kenny EF. The role of neutrophil extracellular traps in rheumatic diseases. Nature Reviews Rheumatology. 2018;467–75.

16. Bonaventura A, Liberale L, Carbone F, Vecchié A, Diaz-Cañestro C, Camici GG, et al. The pathophysiological role of neutrophil extracellular traps in inflammatory diseases. Thrombosis and Haemostasis. Georg Thieme Verlag. 2018;6–27. https://doi.org/10.1160/TH17-09-0630 PMID: 29304522.
17. Papayannopoulos V. Neutrophil extracellular traps in immunity and disease. Nature Reviews Immunology. 2018;18(2):134–47.
18. Daniel C, Leppkes M, Muñoz LE, Schley G, Schett G, Herrmann M. Extracellular DNA traps in inflammation, injury and healing. Nature Reviews Nephrology. 2019;559–75. https://doi.org/10.1038/s41581-019-0163-2 PMID: 31213698
19. Liew PX, Kubes P. The neutrophil's role during health and disease. Physiological Reviews. 2019;99(2):1223–48.
20. Barnes BJ, Adrover JM, Baxter-Stoltzfus A, Borczuk A, Cools-Lartigue J, Crawford JM, et al. Targeting potential drivers of COVID-19: Neutrophil extracellular traps. Journal of Experimental Medicine. 2020;217(6):e20200652. https://doi.org/10.1084/jem.20200652 PMID: 32302401
21. Bruschi M, Bonanni A, Petretto A, Vaglio A, Pratesi F, Santucci L, et al. Neutrophil extracellular traps profiles in patients with incident systemic lupus erythematosus and lupus nephritis. Journal of Rheumatology. 2020;47(3):377–86.
22. Cahilog Z, Zhao H, Wu L, Alam A, Eguchi S, Weng H, et al. The role of neutrophil NETosis in organ injury: Novel inflammatory cell death mechanisms. Inflammation. Springer. 2020;2021–32.
23. Jariwala MP, Laxer RM. NETosis in Rheumatic Diseases. Current Rheumatology Reports. 2021;23(2):9. https://doi.org/10.1007/s11926-020-00977-6 PMID: 33511473
24. Huang J, Hong W, Wan M, Zheng L. Molecular mechanisms and therapeutic target of NETosis in diseases. MedComm. 2022.
25. Demkow U. Molecular mechanisms of neutrophil extracellular trap (NETs) degradation. Int J Mol Sci. 2023;24(5):4896. https://doi.org/10.3390/ijms24054896 PMID: 36902325
26. Boeltz S, Amini P, Anders H-J, Andrade F, Bilyy R, Chatfield S, et al. To NET or not to NET: current opinions and state of the science regarding the formation of neutrophil extracellular traps. Cell Death & Differentiation. 2019;26(3):395–408.
27. Tan C, Aziz M, Wang P. The vitals of NETs. Journal of Leukocyte Biolog. John Wiley and Sons Inc; 2021;797–808. https://doi.org/10.1002/JLB.3RU0620-375R 33378572
28. Hidalgo A, Libby P, Soehnlein O, Aramburu IV, Papayannopoulos V, Silvestre-Roig C. Neutrophil extracellular traps: from physiology to pathology. Cardiovascular Research. 2022;118(13):2737–53. https://doi.org/10.1093/cvr/cvab329 PMID: 34648022
29. Sil P, Yoo DG, Floyd M, Gingerich A, Rada B. High throughput measurement of extracellular DNA release and quantitative NET formation in human neutrophils in vitro. Journal of Visualized Experiments. 2016;2016(112):52779. https://doi.org/10.3791/52779 PMID: 27404503.
30. Thålin C, Daleskog M, Göransson SP, Schatzberg D, Lasselin J, Laska AC, et al. Validation of an enzyme-linked immunosorbent assay for the quantification of citrullinated histone H3 as a marker for neutrophil extracellular traps in human plasma. Immunologic Research. 2017;65(3):706–12.
31. Rada B. Neutrophil extracellular traps. Methods in Molecular Biology. Humana Press Inc. 2019;517–28.
32. Hayden H, Ibrahim N, Klopf J, Zagrapan B, Mauracher LM, Hell L, et al. ELISA detection of MPO-DNA complexes in human plasma is error-prone and yields limited information on neutrophil extracellular traps formed in vivo. PLOS ONE. 2021;16(4):e0250265. https://doi.org/10.1371/journal.pone.0250265 PMID: 33886636
33. Tian Y, Russo RM, Li Y, Karmakar M, Liu B, Puskarich MA, et al. Serum citrullinated histone H3 concentrations differentiate patients with septic verses non-septic shock and correlate with disease severity. Infection. 2021;49(1):83–93.
34. Tomás-Pérez S, Oto J, Aghababyan C, Herranz R, Cuadros-Lozano A, González-Cantó E, et al. Increased levels of NETosis biomarkers in high-grade serous ovarian cancer patients' biofluids: Potential role in disease diagnosis and management. Frontiers in Immunology. 2023;14:1111344. https://doi.org/10.3389/fimmu.2023.1111344 PMID: 36817483.
35. Rios MR, Garoffolo G, Rinaldi G, Megia-Fernandez A, Ferrari S, Robb CT, et al. A fluorogenic peptide-based smartprobe for the detection of neutrophil extracellular traps and inflammation. Chemical Communications. 2021;57(1):97–100.
36. Bansal S, Sharma V, Gupta R, Singh H, Aggarwal A. A New Approach for Assessment of Neutrophil Extracellular Traps Through Immunofluorescence Staining in Whole Blood Smears. Bio-protocol. 2024;14(11):e5010. https://doi.org/10.21769/BioProtoc.5010 PMID: 38873014.
37. Morimont L, Dechamps M, David C, Bouvy C, Gillot C, Haguet H, et al. NETosis and nucleosome biomarkers in septic shock and critical COVID-19 patients: an observational study. Biomolecules. 2022;12(8):1038. https://doi.org/10.3390/biom12081038 PMID: 36008932.
38. Rahimi MH, Bidar F, Lukaszewicz AC, Garnier L, Payen-Gay L, Venet F, et al. Association of pronounced elevation of NET formation and nucleosome biomarkers with mortality in patients with septic shock. Annals of Intensive Care. 2023;13(1):102.
39. Su F, Moreau A, Savi M, Salvagno M, Annoni F, Zhao L, et al. Circulating nucleosomes as a novel biomarker for sepsis: a scoping review. Biomedicines. 2024;12(7):1385.
40. Sanchez C, Roch B, Mazard T, Blache P, Dache ZAA, Pastor B, et al. Circulating nuclear DNA structural features, origins, and complete size profile revealed by fragmentomics. JCI Insight. 2021;6(7):e144561. https://doi.org/10.1172/jci.insight.144561 PMID: 33571170.
41. Guo Y, Gao F, Wang Q, Wang K, Pan S, Pan Z, et al. Differentiation of HL-60 cells in serum-free hematopoietic cell media enhances the production of neutrophil extracellular traps. Experimental and Therapeutic Medicine. 2021;21(4):353. https://doi.org/10.3892/etm.2021.9784 PMID: 33732326.

42. Manda-Handzlik A, Bystrzycka W, Wachowska M, Sieczkowska S, Stelmaszczyk-Emmel A, Demkow U, et al. The influence of agents differentiating HL-60 cells toward granulocyte-like cells on their ability to release neutrophil extracellular traps. Immunology and Cell Biology. 2018;96(4):413–25. https://doi.org/10.1111/imcb.12015 PMID: 29380901.

43. Atteberry B, Berman BP, Kelly TK, Cayford J. Understanding the complex chromatin dynamics in primary human neutrophils during PMA-induced NET formation. Front Immunol. 2024;15:1445638. https://doi.org/10.3389/fimmu.2024.1445638 PMID: 39524441

44. Van den Ackerveken P, Lobbens A, Pamart D, Kotronoulas A, Rommelaere G, Eccleston M, et al. Epigenetic profiles of elevated cell free circulating H3.1 nucleosomes as potential biomarkers for non-Hodgkin lymphoma. Scientific Reports. 2023;13(1):16335.

45. Papayannopoulos V, Metzler KD, Hakkim A, Zychlinsky A. Neutrophil elastase and myeloperoxidase regulate the formation of neutrophil extracellular traps. Journal of Cell Biology. 2010;191(3):677–91.

46. Gonzalez AS, Bardoel BW, Harbort CJ, Zychlinsky A. Induction and quantification of neutrophil extracellular traps. Methods in Molecular Biology. 2014;1124:307–18.

47. Brinkmann V, Abed UA, Goosmann C, Zychlinsky A. Immunodetection of NETs in paraffin-embedded tissue. Frontiers in Immunology. 2016;7(NOV):513. https://doi.org/10.3389/fimmu.2016.00513 PMID: 27920776.

48. Carmona-Rivera C, Kaplan MJ. Induction and quantification of NETosis. Current Protocols in Immunology. 2016;2016:4.41.1-14.41.14.

49. Masuda S, Shimizu S, Matsuo J, Nishibata Y, Kusunoki Y, Hattanda F, et al. Measurement of NET formation in vitro and in vivo by flow cytometry. Cytometry Part A. 2017;91(8):822–9.

50. Matta B, Battaglia J, Barnes BJ. A new methodology for the quantification of neutrophil extracellular traps in patient plasma. Bio-protocol. 2023;13(12):e4701. https://doi.org/10.21769/BioProtoc.4701 PMID: 37397793.

51. van Breda SV, Vokalova L, Neugebauer C, Rossi SW, Hahn S, Hasler P. Computational Methodologies for the in vitro and in situ Quantification of Neutrophil Extracellular Traps. Frontiers in Immunology. 2019;10:1562. https://doi.org/10.3389/fimmu.2019.01562 PMID: 31354718.

52. Mohanty T, Sørensen OE, Nordenfelt P. NETQUANT: Automated Quantification of Neutrophil Extracellular Traps. Frontiers in Immunology. 2018;8:1999. https://doi.org/10.3389/fimmu.2017.01999 PMID: 29379509.

53. Matta B, Battaglia J, Barnes BJ. Detection of neutrophil extracellular traps in patient plasma: method development and validation in systemic lupus erythematosus and healthy donors that carry IRF5 genetic risk. Frontiers in Immunology. 2022;13:951254. https://doi.org/10.3389/fimmu.2022.951254 PMID: 35958624.

54. Kano H, Aminul Huq M, Tsuda M, Noguchi H, Takeyama N. Sandwich ELISA for Circulating Myeloperoxidase- and Neutrophil Elastase-DNA Complexes Released from Neutrophil Extracellular Traps. Advanced Techniques in Biology & Medicine. 2017;5(01).

55. Wang Y, Li M, Stadler S, Correll S, Li P, Wang D, et al. Histone hypercitrullination mediates chromatin decondensation and neutrophil extracellular trap formation. Journal of Cell Biology. 2009;184(2):205–13. https://doi.org/10.1083/jcb.200806072 PMID: 19153223

56. Yoo D g, Winn M, Pang L, Moskowitz SM, Malech HL, Leto TL. Release of cystic fibrosis airway inflammatory markers from Pseudomonas aeruginosa –stimulated human neutrophils involves NADPH oxidase-dependent extracellular DNA trap formation. The Journal of Immunology. 2014;192(10):4728–38.

57. Li M, Lin C, Leso A, Nefedova Y. Quantification of Citrullinated Histone H3 Bound DNA for Detection of Neutrophil Extracellular Traps. Cancers. 2020;12(11):3424. https://doi.org/10.3390/cancers12113424 PMID: 33218159

58. Konig MF, Andrade F. A Critical Reappraisal of Neutrophil Extracellular Traps and NETosis Mimics Based on Differential Requirements for Protein Citrullination. Front Immunol. 2016;7. https://doi.org/10.3389/fimmu.2016.00461

59. de Bont CM, Koopman WJH, Boelens WC, Pruijn GJM. Stimulus-dependent chromatin dynamics, citrullination, calcium signalling and ROS production during NET formation. Biochimica et Biophysica Acta - Molecular Cell Research. 2018;1865(11):1621–9.

60. Parker H, Winterbourn CC. Reactive oxidants and myeloperoxidase and their involvement in neutrophil extracellular traps. Frontiers in Immunology. 2013;3:424. https://doi.org/10.3389/fimmu.2012.00424 PMID: 23346086.

61. Kinkade JM, Pember SO, Barnes KC, Shapira R, Spitznagel JK, Martin LE, et al. Differential distribution of distinct forms of myeloperoxidase in different azurophilic granule subpopulations from human neutrophils. Biochemical and Biophysical Research Communications. 1983;114(1):296–303.

62. Van den Ackerveken P, Hannart C, Pamart D, Varsebroucq R, Wargnies M, Thiry O, et al. High-throughput epigenetic profiling immunoassays for accelerated disease research and clinical development. bioRxiv. 2024. https://doi.org/2024.12.05.626944

63. Tilley DO, Abuabed U, Arndt UZ, Schmid M, Florian S, Jungblut PR, et al. Histone H3 clipping is a novel signature of human neutrophil extracellular traps. eLife. 2022;11:1–61.

64. Garrido MM, Ribeiro RM, Krüger K, Pinheiro LC, Guimarães JT, Holdenrieder S, et al. Relevance of Circulating Nucleosomes, HMGB1 and sRAGE for Prostate Cancer Diagnosis. In Vivo. 2021;35(4):2207–12. https://doi.org/10.21873/invivo.12492 PMID: 34182498

65. Zukas K, Cayford J, Serneo F, Atteberry B, Retter A, Eccleston M, et al. Rapid high-throughput method for investigating physiological regulation of neutrophil extracellular trap formation. J Thromb Haemost. 2024;22(9):2543–54. https://doi.org/10.1016/j.jtha.2024.05.028 PMID: 38866247

66. Thålin C, Aguilera K, Hall NW, Marunde MR, Burg JM, Rosell A, et al. Quantification of citrullinated histones: development of an improved assay to reliably quantify nucleosomal H3Cit in human plasma. Journal of Thrombosis and Haemostasis. 2020;18(10):2732–43. https://doi.org/10.1111/jth.15003 PMID: 32654410